Available online at www.sciencedirect.com
SCIENCE DIRECT®
Precambrian Research 123 (2003) 67–80
Precambrian Research
www.elsevier.com/locate/precamres

Plutonic and metamorphic rocks from the Keraf Suture (NE Sudan): a glimpse of Neoproterozoic tectonic evolution on the NE margin of W. Gondwana

T. Bailo [a,1], H. Schandelmeier [a], G. Franz [a], Chih-Hsien Sun [b,2], R.J. Stern [b,*]

[a] *Institut für Angewandte Geowissenschaften, Technische Universität Berlin, D-10623 Berlin, Germany*
[b] *Geosciences Department, University of Texas at Dallas, Box 830688, Richardson, TX 75083-0688, USA*

Received 21 March 2002; accepted 5 February 2003

Abstract

The Keraf Shear Zone (KSZ) of NE Sudan formed in Neoproterozoic time when juvenile crust of the Arabian–Nubian Shield collided with reworked older crust of the Saharan Metacraton. Orthogneisses and deformed granitoids which intrude carbonate sediments are calc-alkaline, medium-K, metaluminous and I-type diorites and granodiorites, with subduction-related trace element signatures. $^{207}Pb/^{206}Pb$ zircon single grain ages are ~730 Ma for the high-grade gneiss and ~710 Ma for granitoids. K/Ar ages are 660 Ma for hornblende from the granitoids and 560 Ma for biotite from the high-grade gneiss and the plutons. The geochronologic data indicate that the crust formed ~730–710 Ma and that orogenic activity ended by ~565 Ma. Cooling occurred over much of NE Africa at about the same time, possibly caused by orogenic collapse or unroofing caused by extensive glaciation. Pb isotopic ratios indicate an oceanic source for both the magmatic and metamorphic rocks in the KSZ. Sm/Nd model ages are 620–770 Ma for the post-tectonic plutons and 830–900 Ma for the gneiss, indicating negligible involvement of a pre-Neoproterozoic material in the evolution of Keraf igneous rocks. The $(^{87}Sr/^{86}Sr)_i$ values range from 0.7026 to 0.7046, which are indistinguishable from initial ratios for juvenile crust of the Arabian Nubian Shield and are lower than initial Sr isotopic compositions for the Saharan Metacraton. The isotopic data indicate that Keraf igneous rocks are juvenile additions to the crust and that the boundary between the Saharan Metacraton and the Arabian–Nubian Shield lies to the west.

Keywords: Neoproterozoic; Arabian–Nubian Shield; Granitoids; Isotopic compositions; Geochronology

1. Introduction

The most important tectonic events of Neoproterozoic time are related to the break-up of the Rodinia supercontinent sometime around 800 Ma followed by the formation of a supercontinent, known variously as Pannotia (Dalziel, 1997) or Greater Gondwanaland (Stern, 1994) at the end of Neoprotoerozoic time. A critical aspect in the formation of the

* Corresponding author. Tel.: +1-972-883-2442; fax: +1-972-883-2537.
E-mail addresses: bailo26@hotmail.com (T. Bailo), rjstern@utdallas.edu (R.J. Stern).
[1] Present address: 8000 East 12th Avenue, B8-A6, Denver, CO 80220, USA.
[2] Present address: Exploration and Development Research Institute, Chinese Petroleum Corporation, P.O. Box 166, Miaoli, Taiwan, ROC.

0301-9268/03/$ – see front matter © 2003 Elsevier Science B.V. All rights reserved.
doi:10.1016/S0301-9268(03)00044-5

end-Neoproterozoic supercontinent was the collision of juvenile arc terranes of the Arabian–Nubian Shield with palimpsest older continental crust now preserved in the Saharan Metacraton of N. Africa (Fig. 1A). In contrast to the generally low-grade and isotopically juvenile sequences of the Arabian–Nubian Shield (Stern, 2002), the Saharan Metacraton contains abundant higher-grade metamorphic rocks which commonly show ages or isotopic signatures indicating that it is dominated by older crust reworked during Neoproterozoic time (Abdelsalam et al., 2002). Understanding the Keraf Shear Zone (KSZ) in NE Sudan is important for understanding formation of the end-Neoproterozoic supercontinent, because this may be the site of a continent-ocean suture between the Saharan Metacraton to the west and juvenile arc terranes of the Red Sea Hills to the east (Fig. 1A; Abdelsalam and Stern, 1996a,b; Abdelsalam et al., 1998). This fundamental crustal boundary approximately controls the course of the Nile in Egypt and farther south in Sudan and so is covered by Phanerozoic sediments, but in N. Sudan the Nile jogs far to the west (Fig. 1B). This is where the Keraf Shear Zone is exposed and is the focus of our study.

The KSZ is a N–S trending, ophiolite-decorated structural belt that was first recognized by Almond and Ahmed (1987). Thick and deformed carbonate sequences and ophiolites that strike parallel to the KSZ are further evidence that this approximates an important crustal boundary. The KSZ, where exposed, is ∼500 km-long belt that is thrust-bounded and wedge-shaped belt. The KSZ is narrower (∼30 km) in the south than it is in the north (∼150 km; Fig. 1B). The wedge-shape geometry reflects N–S variations in styles of deformation, metamorphism, and uplift. Although several stages of deformation have been identified in the evolution of the KSZ, timing is constrained only by $^{40}Ar/^{39}Ar$ ages of 577 Ma for two biotite and one hornblende samples from a late-stage deformed granite associated with a NNW-trending sinistral shear zone south of Abu Hamed (Abdelsalam et al., 1998). These are cooling ages corresponding to the end of the orogenic cycle.

Traverses across the central sector of the KSZ reveal that these rocks are dominated by high- to medium-grade gneiss, siliciclastic and carbonate-rich metasediments (Baileteb Group) intercalated with sills of metabasalt and microdiorite, ophiolitic nappes, molasse-type sediments and post-tectonic granitoids (Fig. 2). Metasediments in the KSZ south of the study area are mostly metamorphosed to amphibolite facies. Rocks in the northern KSZ are less metamorphosed and better preserve primary features. Sedimentary structures and textures in the low-grade units indicate that some were deposited in shallow water and others appear to be turbidites deposited in relatively deep water, perhaps on a continental slope (Abdelrahman, 1993; Abdelsalam and Stern, 1996b). The time of sedimentation was inferred by Stern et al. (1993) on the basis of C and Sr isotopes to have occurred about 750 Ma. Keraf ophiolites have most of the lithological characteristics of Phanerozoic ophiolites and outcrop as N–S trending fault-bounded ridges. Deformed rocks of the KSZ are locally overlain by molasse-type sediments, including unmetamorphosed polymict conglomerate, sandstones and volcanic tuffs; these are not present in the area shown in Fig. 2. Granitoids are widespread and include deformed diorites and granodiorites—the focus of our geochemical and isotopic studies—as well as post-tectonic granites.

Form, geometry and kinematic evolution of KSZ structures indicate a four-phase transpressive deformation. Shearing was associated with instantaneous strains of unknown orientations, but the finite strain state was clearly characterized by E–W horizontal shortening, sinistral shearing along N–S trending faults, and vertical extension, indicating crustal thickening. The structural evolution of the KSZ has been outlined in a series of papers by Abdelsalam and co-workers (Abdelsalam et al., 1998; Abdelsalam and Stern, 1996a,b). The tectonic history of the shear zone reflects closure of the Mozambique Ocean and collision of the Wadi Halfa–Bayuda Terrane (Saharan Metacraton) against the Gabgaba Terrane (Arabian–Nubian Shield) (Fig. 1B).

In this study, we present chemical, geochronologic and isotopic compositional data for a suite of deformed diorites, granodiorites, and gneisses in the KSZ. We use this data to characterize the magmatic evolution of the Keraf igneous rocks; constrain the age of the Keraf passive margin sequence, and help in understanding the relationship between older crust of the Saharan Metacraton to the west and juvenile crust of the Arabian–Nubian Shield to the east.

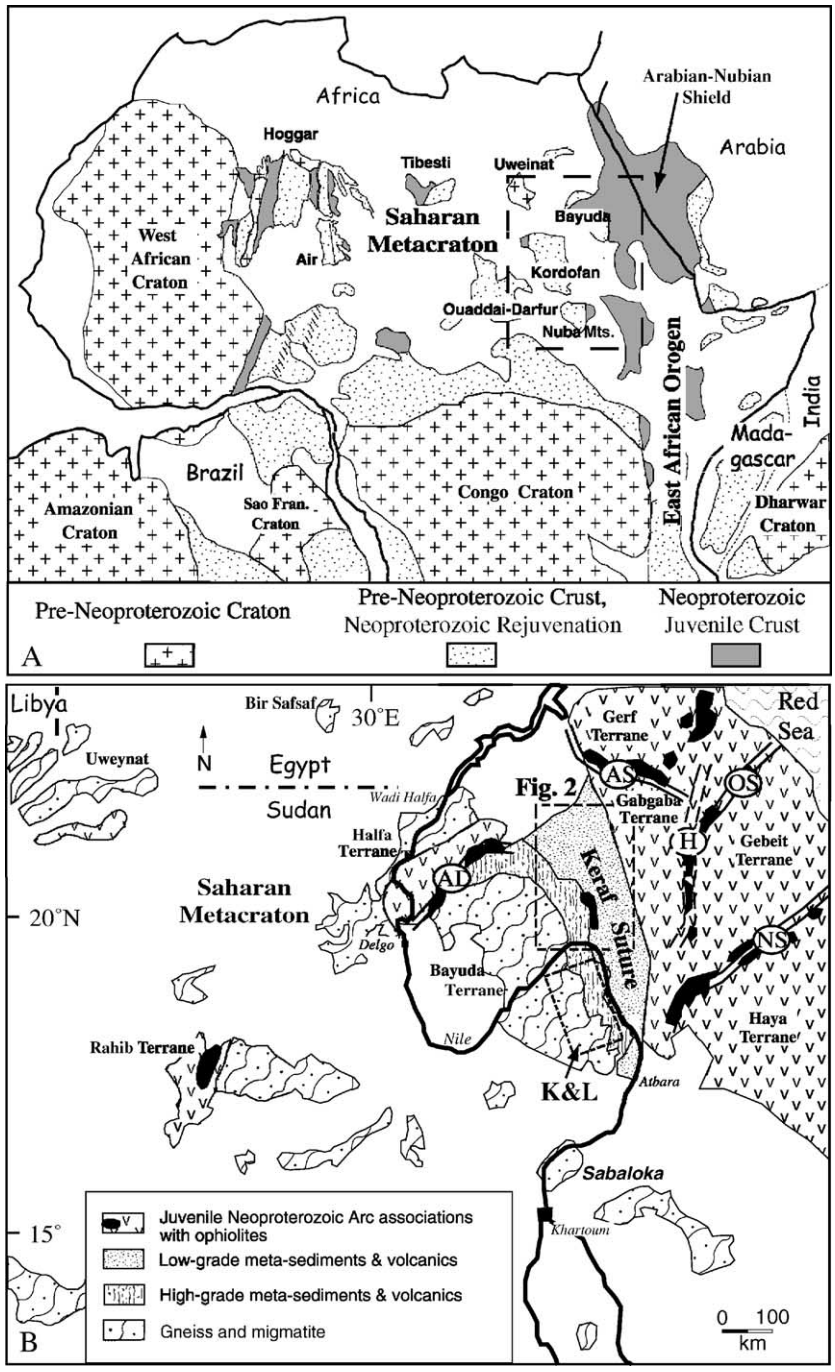

Fig. 1. (A) Locality map for central Gondwanaland, modified after Küster and Liegeois (2001). Dashed box shows the location of (B). (B) Locality map for NE Sudan and SE Egypt, modified after Küster and Liegeois (2001). Letters in ovals denote important suture zones: AD, Atmur–Delgo Suture; AS, Allaqi–Heiani Suture; OS, Onib–Sol Hamed Suture; NS, Nakasib Suture. H enclosed by dashed oval is Hamisana Shear Zone. Dashed box labeled 'K&L' is the study area of Küster and Liegeois (2001). Location of area of detail shown in Fig. 2 is shown by the northern dashed rectangle.

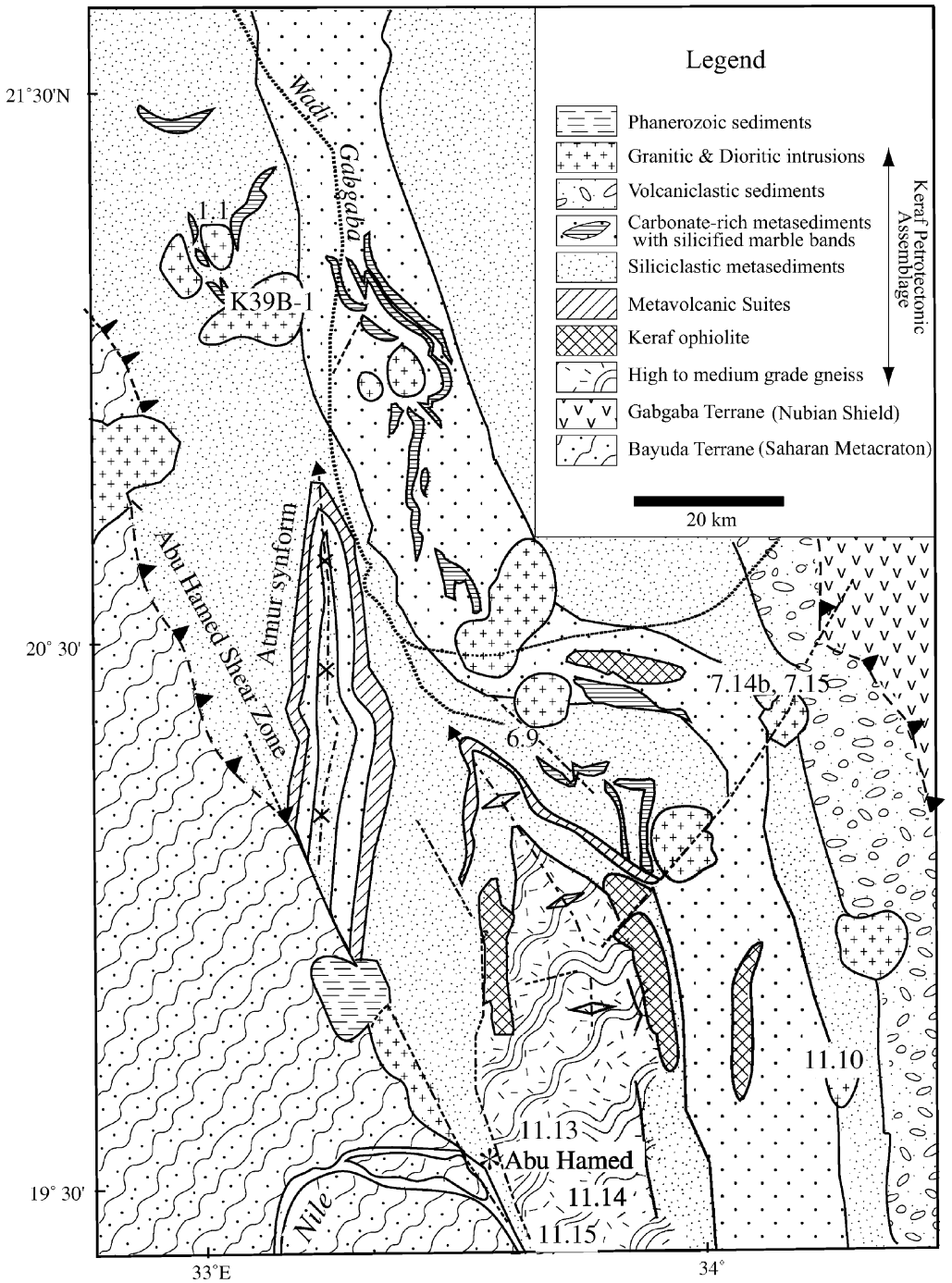

Fig. 2. Detailed study area with sample locations.

Table 1
Geochemistry of granitic plutons and gneiss

	Sample							
	1.1	K39B-1	6.9	7.14b	7.15	7.15a	11.10	11.15
SiO_2 (%)	52.00	55.98	70.72	54.74	66.87	66.90	69.51	67.13
Al_2O_3	17.60	19.52	15.85	13.84	15.88	17.16	14.82	14.95
Fe_2O_3	7.13	5.96	2.26	7.16	2.96	3.21	3.57	3.6
MnO	0.118	0.080	0.046	0.084	0.026	0.040	0.067	0.036
MgO	5.93	3.31	0.55	4.77	1.64	1.24	0.51	1.93
CaO	10.41	6.64	2.74	7.69	4.06	4.01	2.39	4.19
Na_2O	2.99	4.27	4.17	3.06	5.09	4.99	3.86	4.2
K_2O	0.62	1.64	2.36	1.09	1.36	1.43	3.49	1.46
TiO_2	1.19	1.33	0.36	0.96	0.46	0.48	0.44	0.55
P_2O_5	0.214	0.43	0.118	0.420	0.176	0.143	0.170	0.219
L.O.I	1.57	1.81	0.67	4.84	0.84	0.79	0.94	0.76
SUM	99.77	100.97	99.84	98.65	99.36	100.39	99.77	99.03
Na_2O/K_2O	4.82	2.60	1.77	2.81	3.74	3.49	1.11	2.88
Mg#	0.62	0.52	0.32	0.57	0.52	0.43	0.22	0.51
As ppm	b.d.l.		7	<7	14	5	6	11
Ba	157	344	1080	290	419	495	780	424
Ce	32	72	94			56	80	
Cr	247		15	59	<10	14	12	15
Cu	42		<10	<4	23	23	11	42
Dy	3.2		1.7		1.1		6.7	
Er	1.5		0.9		0.6		4.5	
Eu	1.4		0.9		0.8		1.8	
Ga	15	14	26	18	20	26	24	16
Gd	1.6		2.6		1.6		6.5	
Hf	4		3.3	b.d.l.	3	4	8.1	
Ho	0.6				0.2			
La	12.5		31.4		11.0		32.9	
Lu	0.2		0.1		0.1	0.10	0.6	
Nb	5	11	4	b.d.l.	3	b.d.l.	6	
Nd	19.6	33.7	30.4	60	8.5	<10	44	
Ni	89		<8	24	<10	9	<8	13
Pb	<10	13	<10	<10	<10	b.d.l.	<10	
Pr	2.7		6		2.2		9.3	3.5
Rb	6.2	25.7	19.7	21	24	31	80	39
Sb	<3		4	4.8	3.9	5	4.8	
Sc	26	10	<10	b.d.l.	b.d.l.	<10	<10	
Sm	4.8	6.2	4.48	b.d.l.	2.1	b.d.l.	8.4	
Sr	645	986	639	490	643	703	252	295
Th	b.d.l.	6	<5	b.d.l.	<8.0	b.d.l.	6	
Tl	b.d.l.		<2.5	b.d.l.	<2.5	<2.5	<2.5	
V	189	177	43	158	55	71	36	64
Y	19	15	<10			10	39	
Yb	1.6		0.8		0.6	0.6	4	
Zn	54		49	67	40	52	77	39
Zr	132	106	153	141	142	161	299	67
Sr/Y	33.9	65.7				70.3	6.5	
K/Rb	830.0	529.6	994.3	430.8	470.3	382.9	362.1	310.7
Sr/Nd	32.91	29.26	21.02	8.17	7.56		5.73	

b.d.l.: below detection limits.

Table 2
Pb isotopic analyses of zircon grains

Sample	Grain	$^{207}Pb/^{206}Pb$	$^{204}Pb/^{206}Pb$	$^{207}Pb/^{206}Pb$ correction	Scan	Age (Ma)	Mean age (Ma)
1.1	1	$0.07453 \pm 2.87 \times 10^{-4}$	$8.3 \times 10^{-4} \pm 1.97 \times 10^{-5}$	$0.062892 \pm 1.47 \times 10^{-4}$	90	704.5 ± 5	
	2	$0.070816 \pm 2.0 \times 10^{-4}$	$5.57 \times 10^{-4} \pm 1.46 \times 10^{-5}$	$0.063074 \pm 1.31 \times 10^{-4}$	90	710.7 ± 4.4	
	3	$0.063888 \pm 2.87 \times 10^{-4}$	$4.96 \times 10^{-5} \pm 8.15 \times 10^{-6}$	$0.063407 \pm 2.88 \times 10^{-4}$	90	721.8 ± 9.6	
	4	$0.063978 \pm 8.04 \times 10^{-5}$	$6.07 \times 10^{-5} \pm 3.27 \times 10^{-6}$	$0.063338 \pm 8.23 \times 10^{-5}$	90	719.0 ± 2.8	714 ± 7
6.9	1	$0.064374 \pm 1.64 \times 10^{-4}$	$1.09 \times 10^{-4} \pm 5.42 \times 10^{-6}$	$0.063038 \pm 1.86 \times 10^{-4}$	90	709.5 ± 5.7	
	2–4	$0.0658121 \pm 7.30107 \times 10^{-5}$	$2.163 \times 10^{-4} \pm 3.19758 \times 10^{-6}$	$0.06295 \pm 4.41075 \times 10^{-5}$	90	706.4 ± 2.6	
	3 & 6	$0.064891 \pm 8.36 \times 10^{-5}$	$1.43 \times 10^{-4} \pm 2.91 \times 10^{-6}$	$0.063079 \pm 8.41 \times 10^{-5}$	90	710.9 ± 2.8	
	7–13	$0.0648173 \pm 5.67811 \times 10^{-5}$	$1.212 \times 10^{-4} \pm 1.75163 \times 10^{-6}$	$0.06332 \pm 5.76853 \times 10^{-5}$	90	718.7 ± 1.4	711 ± 5
11.13	1	$0.071912 \pm 3.25 \times 10^{-4}$	$5.88 \times 10^{-4} \pm 2.4 \times 10^{-5}$	$0.063746 \pm 3.06 \times 10^{-4}$	90	733.1 ± 10.1	
	2	$0.071066 \pm 3.95 \times 10^{-4}$	$5.26 \times 10^{-4} \pm 2.13 \times 10^{-5}$	$0.063779 \pm 2.62 \times 10^{-4}$	90	734.3 ± 8.7	
	3 & 4	$0.067429 \pm 1.27 \times 10^{-4}$	$2.5 \times 10–4 \pm 1.09 \times 10^{-5}$	$0.064094 \pm 1.35 \times 10^{-4}$	90	744.7 ± 4.5	
	5 & 6	$0.066025 \pm 1.51 \times 10^{-4}$	$1.72 \times 10^{-4} \pm 6.79 \times 10^{-6}$	$0.063804 \pm 1.3 \times 10^{-4}$	90	735.0 ± 4.3	737 ± 5
11.14	1	$0.066241 \pm 2.39 \times 10^{-4}$	$1.36 \times 10^{-4} \pm 1.03 \times 10^{-5}$	$0.064534 \pm 2.38 \times 10^{-4}$	90	759.1 ± 7.8	
	2	$0.071125 \pm 2.43 \times 10^{-4}$	$4.96 \times 10^{-4} \pm 1.75 \times 10^{-5}$	$0.064279 \pm 2.45 \times 10^{-4}$	90	750.8 ± 8.1	
	3	$0.070207 \pm 4.95 \times 10^{-4}$	$4.88 \times 10^{-4} \pm 2.54 \times 10^{-5}$	$0.063456 \pm 3.63 \times 10^{-4}$	18	723.5 ± 12.2	
	4 & 5	$0.067235 \pm 2.43 \times 10^{-4}$	$3.17 \times 10^{-4} \pm 1.43 \times 10^{-5}$	$0.062924 \pm 1.42 \times 10^{-4}$	42	705.6 ± 4.8	
	6–8	$0.0645268 \pm 1.23127 \times 10^{-4}$	$8.723 \times 10^{-5} \pm 5.50522 \times 10^{-6}$	$0.06351 \pm 1.23482 \times 10^{-4}$	90	725.3 ± 4.2	733 ± 18

2. Samples

Five granitic plutons and a large body of orthogneiss were sampled, at locations shown in Fig. 2. Sample 1.1 is from a plagioclase–hornblende–quartz–chlorite–epidote–muscovite diorite. Sample K-39B-1 is from a larger mass of hornblende diorite slightly farther south. Sample 6.9 is from a plagioclase (zoned)–hornblende–K-feldspar–quartz (myrmekite)–muscovite granodiorite. Samples 7.14b and 7.15 are from the same diorite–granodiorite pluton, and are composed of plagioclase, quartz, biotite, hornblende, epidote ± muscovite, ±chlorite. Sample 11.10 is a quartz–K-feldspar–plagioclase–biotite granite. Samples 11.13, 11.14, and 11.15 are from an extensive body of orthogneiss in the southern part of the study area. The gneiss has been metamorphosed to upper amphibolite facies and was affected by the earliest deformational events of the KSZ. Sample 11.13 consists of quartz, plagioclase, biotite, K-feldspar, and garnet, 11.14 of plagioclase, quartz, biotite, muscovite, hornblende, and garnet, and 11.15 of plagioclase, quartz, biotite, hornblende, epidote, and chlorite. All of the plutons which we have dated intrude the metasedimentary sequence and are affected by the N–S foliation, inferred to have formed at the time of suturing. These plutons were emplaced prior to Keraf tectonism although they do not have the same complicated structures as the gneiss. The relationship of the gneisses to the metasediments is not clear, but we suspect that the orthogneisses represent highly deformed plutons emplaced deep in the crust and may post-date deposition of the metasediments.

3. Methods and analytical techniques

Major oxide and trace element compositions were determined using the X-ray fluorescence (XRF) spectrometer at TU Berlin. Analyses are listed in Table 1. The inductively coupled plasma (ICP) emission spectrometer at TU Berlin was used to determine REE abundances for selected samples. Detection limits for the ICP technique is 0.1 ppm. Zircon single grain dating for four samples was conducted at the Bergakademie TU Freiberg. The method used and the operating parameters are outlined in Kober (1986, 1987). Results are listed in Table 2. Biotite and hornblende K/Ar dating was carried out at the Institut für Geologie und Dynamik der Lithosphere in Göttingen. Results and operating parameters are given in Table 3. Pb isotopic compositions for K-feldspar and Sr and Nd isotopic ratios for whole rock samples were determined at the University of Texas at Dallas (Tables 4–6). Rb and Sr contents were determined for some samples by isotope dilution and $^{87}Sr/^{86}Sr$ was determined using the Finnigan MAT 261 solid-source mass spectrometer at UTD. Reproducibility of $^{87}Sr/^{86}Sr$ is ±0.00004. During the course of this work the UTD lab obtained a mean $^{87}Sr/^{86}Sr = 0.70803 \pm 3$ for multiple analyses of the E&A $SrCO_3$ standard; data reported here have been adjusted to $^{87}Sr/^{86}Sr = 0.70800$ for the E&A standard. Initial $^{87}Sr/^{86}Sr$ was calculated using measured $^{87}Sr/^{86}Sr$ and Rb and Sr concentrations determined by isotope dilution, and zircon ages except for K39B-1, for which an age of 700 Ma was assumed. Nd and Sm concentrations for some samples and $^{143}Nd/^{144}Nd$ were also determined using the UTD Finnigan-MAT261. Uncertainties on Sm/Nd measurements are about 1%. Calculations of $\varepsilon_{Nd(t)}$ were made assuming Bulk Earth $^{143}Nd/^{144}Nd = 0.1967$ and using values of ε_{Nd} for the UCSD standard (−15.2) and BCR (−0.16; Pier et al., 1989). A total range of ±0.00002 observed for $^{143}Nd/^{144}Nd$ of the standard (mean value = 0.511855) and is taken as the analytical uncertainty for the samples. K-feldspars to be analyzed for Pb isotopes were rinsed in 6 N HCl, then leached overnight in 1% HF. Pb was isolated by an anion exchange column procedure followed by the single bead technique. The analysis was corrected for 0.15% per

Table 3
K–Ar geochronology results

Sample	Mineral	K_2O (wt.%)	^{40}Ar (nl/g)	^{40}Ar (%) (radiogenic)	Age (Ma)	2σ-error (Ma)	2σ-error (%)
1.1	Hornblende	0.46	11.77	87.71	658.0	24.0	3.6
6.9	Biotite	9.52	202.95	99.65	563.5	11.5	2.0
11.13	Biotite	9.57	204.69	99.10	565.1	11.7	2.0
11.14	Biotite	9.35	200.21	99.62	565.6	12.9	2.3

Table 4
Rb–Sr isotopic data

Sample	Rb (ppm)	Sr (ppm)	$^{87}Rb/^{86}Sr$	$(^{87}Sr/^{86}Sr)_m$	$(^{87}Sr/^{86}Sr)_i$
1.1	6.2	645	0.028	0.70304	0.70275
K39B-1	25.7	986	0.0754	0.70356	0.70281[a]
6.9	19.7	639	0.089	0.70549	0.70459
11.13	18.2	477	0.110	0.70437	0.70322
11.14	8.0	538	0.043	0.70343	0.70298

[a] Assuming age = 700 Ma.

Table 5
Sm–Nd isotopic data

Sample	Sm (ppm)	Nd (ppm)	$^{147}Sm/^{144}Nd$	$^{143}Nd/^{144}Nd$	$\varepsilon_{Nd(t)}$	T_{DM} (Ga)
1.1	4.8	19.6	0.1481	0.512781	7.3	0.62
K39B-1	6.25	33.7	0.1121	0.512546	5.9[a]	0.75
6.9	4.48	30.4	0.0891	0.512418	5.6	0.77
11.13	0.62	3.1	0.1209	0.512497	4.5	0.90
11.14	0.36	2.43	0.0896	0.512369	4.9	0.83

[a] Assuming age = 700 Ma.

Table 6
Pb isotopic data for K-feldspars

Sample	$^{206}Pb/^{204}Pb$	$^{207}Pb/^{204}Pb$	$^{208}Pb/^{204}Pb$
6.9	18.065	15.562	37.462
11.13	17.599	15.500	37.107
11.14	17.516	15.481	37.072

amu fractionation. Six analyses of the SRM-981 standard during the course of this work yielded the following lead isotopic composition: $^{206}Pb/^{204}Pb = 16.946$, $^{207}Pb/^{204}Pb = 15.501$, and $^{208}Pb/^{204}Pb = 36.756$.

4. Results

The samples are characterized by an extended range of SiO_2 (52–71 wt.%) and are mainly a medium-K suite (Fig. 3A). The dioritic samples (1.1, K39B-1, and 7.14b) are dominantly mantle melts, with Mg# (=molar Mg/Mg + Fe) of 0.52–0.62, up to 89 ppm Ni and up to 247 ppm Cr (Table 1). All but the most siliceous samples (11.10 and 6.9) have $Na_2O/K_2O >$ 2.5. The plutonic rocks are characterized by Alumina Saturation Index (ASI: molar $Al_2O_3/CaO + Na_2O + K_2O$) less than 1.1, and are meta-aluminous. On the AFM diagram (Irvine and Baragar, 1971) the samples define a calc-alkaline trend. The suite has moderate to high K/Rb (300–1000). Some of the samples have high Sr/Y (up to 70), suggesting affinities with adakites (Drummond and Defant, 1990). The REE patterns are steep and generally lack Eu-anomalies (Fig. 3B). The samples analyzed for Rb, Y and Nb fall in fields for volcanic arc granitoids (Fig. 3C; Pearce et al., 1984). The observed depletion of Nb compared to the LREE and Th is typical of subduction-related granitoids (Condie, 1998). We conclude that KSZ granitoids have most of the characteristics of I-type granitoids (Condie, 1998; Küster and Harms, 1998).

Results of $^{207}Pb/^{206}Pb$ zircon evaporation method applied to two plutons (1.1, 6.9) and two samples of the large body of orthogneiss east of Abu Hamed (11.13, 11.14) are listed in Table 2. Three hundred and sixty scans for each of the plutonic samples yielded relatively well-constrained ages of 714±7 and 711±5 Ma, interpreted as approximating the time of intrusion. All zircon grains separated from the gneiss are euhedral and small to medium in size with no obvious overgrowths. Therefore, the zircon ages are considered as the ages of the high-grade metamorphism (upper amphibolite–granulite facies) in the Keraf area or crystallization of the igneous protolith. Zircons from

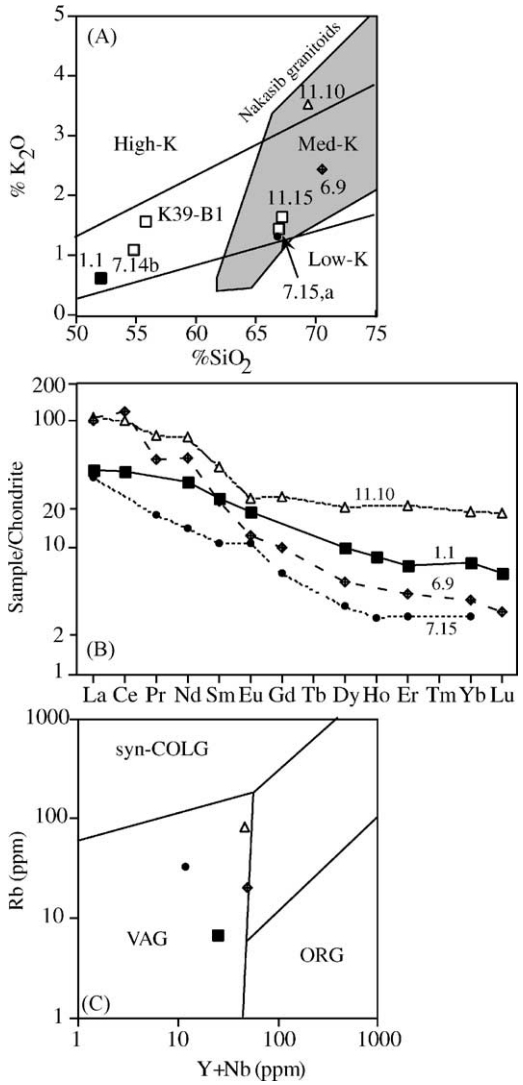

Fig. 3. Geochemical variations of Keraf rocks. (A) Potassium–silica diagram. Gray field encloses compositions of ~700–830 Ma intrusions into the Nakasib Suture, reported by Stern and Abdelsalam (1998). (B) Chondrite-normalized REE patterns; (C) discriminant diagrams (symbols are the same as in B) from Pearce et al. (1984). ORG, ocean-ridge granite; syn-COLG, syn-collisional granite; VAG, volcanic arc granite.

sample 11.13 yielded 360 scans and a relatively well-constrained age of 737 ± 5 Ma, whereas those from 11.14 yielded 330 scans and an age of 737 ± 18 Ma.

K/Ar analytical data for hornblende and biotite separated from four samples are listed in Table 3. Hornblende from sample 1.1 yields an age of 658 ± 24 Ma, interpreted to reflect the last time of cooling below ~525 °C (Harrison, 1981). Electron microprobe analysis data indicate that the hornblende has rims and inclusions of secondary minerals such as epidote and actinolite. Thus, the hornblende age could be partially reset and the age could be intermediate between the crystallization age of the hornblende and the metamorphic overprint responsible for the secondary minerals. Ages of biotite from both plutons and gneiss are remarkably similar, between 563 and 566 Ma, although with analytical uncertainties of 11–13 Ma. Because biotites effectively close to loss of Ar below ~325 °C (Harrison et al., 1985), these results indicate that the KSZ had cooled to ~325 °C by ~565 Ma.

Initial $^{87}Sr/^{86}Sr$ values are reported for five samples (two gneiss and three plutonic intrusions) (Table 4). All five samples have abundant Sr (477–986 ppm) and low $^{87}Rb/^{86}Sr$ (0.11 or less), so the correction of $^{87}Sr/^{86}Sr$ for radiogenic growth is insensitive to uncertainties in age and Rb/Sr. The $(^{87}Sr/^{86}Sr)_i$ values for four of the samples fall in the interval 0.70275–0.70322, with one sample (6.9) showing a significantly higher value of 0.70459. The $(^{87}Sr/^{86}Sr)_i$ values are plotted in Fig. 4 and compared with similar results from the Arabian–Nubian Shield and the Saharan Metacraton. The four samples with nonradiogenic Sr are indistinguishable from the initial ratios reported for juvenile crust of the Arabian Nubian Shield and are lower than the ones reported from the Saharan Metacraton. The sample with elevated $(^{87}Sr/^{86}Sr)_i$ is the only sample which contains muscovite, a possible indication of sediment involvement. With this exception, the $(^{87}Sr/^{86}Sr)_i$ values indicate a very short crustal residence time for both magmatic and metamorphic rocks from the KSZ. The relatively higher $(^{87}Sr/^{86}Sr)_i$ value (0.7046) of sample 6.9 may also be due to thermal resetting of isotopic systematics or reflect the involvement of older sediments, crust or heterogeneous lithosphere.

Sm–Nd concentrations and Nd isotopic ratios for five samples from the KSZ are reported in Table 5. Initial Nd data are reported as $\varepsilon_{Nd(t)}$, where t refers to the crystallization age of the rock and ε_{Nd} refers to the isotopic composition of the sample relative to the bulk earth. Keraf samples define a narrow range of $\varepsilon_{Nd(t)}$, i.e. between +4.5 and +7.3 with a mean of +5.6. The plutonic samples (1.1, K39B-1, and 6.9) are characterized by slightly higher $\varepsilon_{Nd(t)}$ (+5.6 to +7.3)

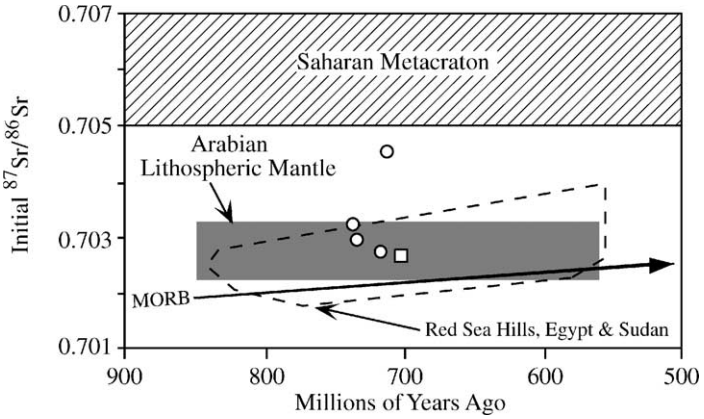

Fig. 4. Strontium evolution diagram. Modified after Stern and Abdelsalam (1998). Open symbols plot $(^{87}Sr/^{86}Sr)_i$ for well-dated samples; open square is for sample K-39B-1 where age is assumed = 700 Ma.

than the gneisses (+4.5 to +4.9). T_{DM} is a model age calculated from the intersection of the sample's radiogenic growth and that of hypothetical depleted mantle (Nelson and DePaolo, 1985), and are sometimes referred to as 'crust formation age'. $^{147}Sm/^{144}Nd$ ranges from 0.09 to 0.15, lower than the cut-off of 0.165 adopted by Stern (2002). This allows calculation of meaningful T_{DM} ages for all five samples. The magmatic rocks have T_{DM} in the range of 0.62–0.77 Ga, which is indistinguishable from the mean crystallization age (710 Ma). The Keraf gneiss has slightly older model ages of 0.83–0.90 Ga (Table 5; Fig. 5A), suggesting longer crustal residence than that of the magmatic rocks. Nevertheless, Nd model ages for all of the Keraf rocks that we have analyzed have a mean of 0.77 Ga, indistinguishable from the mean of 0.76 Ga

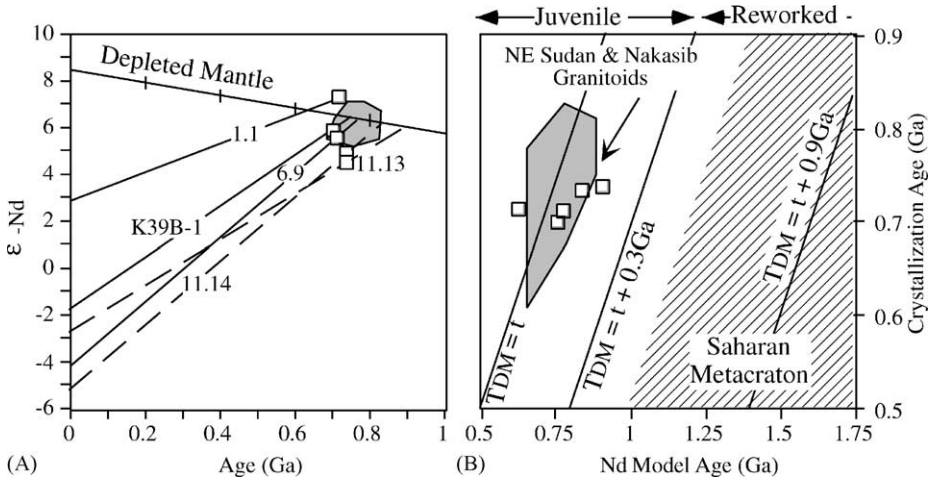

Fig. 5. Nd isotopic systematics for Keraf Shear Zone rocks. (A) Initial Nd isotopic compositions relative to that of the depleted mantle model (Nelson and DePaolo, 1985). Symbols show the initial isotopic composition of Nd in four dated samples. Sample K39B-1 is undated, but yields T_{DM} model age of 0.75 Ga. Note that the $\varepsilon_{Nd(t)}$ of the Keraf plutonic rocks (solid line) is about $\pm 1\varepsilon$ unit of the model depleted mantle, whereas that for the gneisses (dashed line) is 2–3ε units lower than the model depleted mantle. Gray field is for 'NE Sudan & Nakasib Granitoids', from Stern and Abdelsalam (1998). (B) Comparison of crystallization age (t) and T_{DM} model age, after Stern and Abdelsalam (1998). Fields labeled 'NE Sudan & Nakasib Granitoids' and 'Saharan Metaraton' are from Stern and Abdelsalam (1998). Note that Keraf Shear Zone samples fall close to the line $T_{DM} = t$, indicating juvenile crust without discernible contributions from older crust.

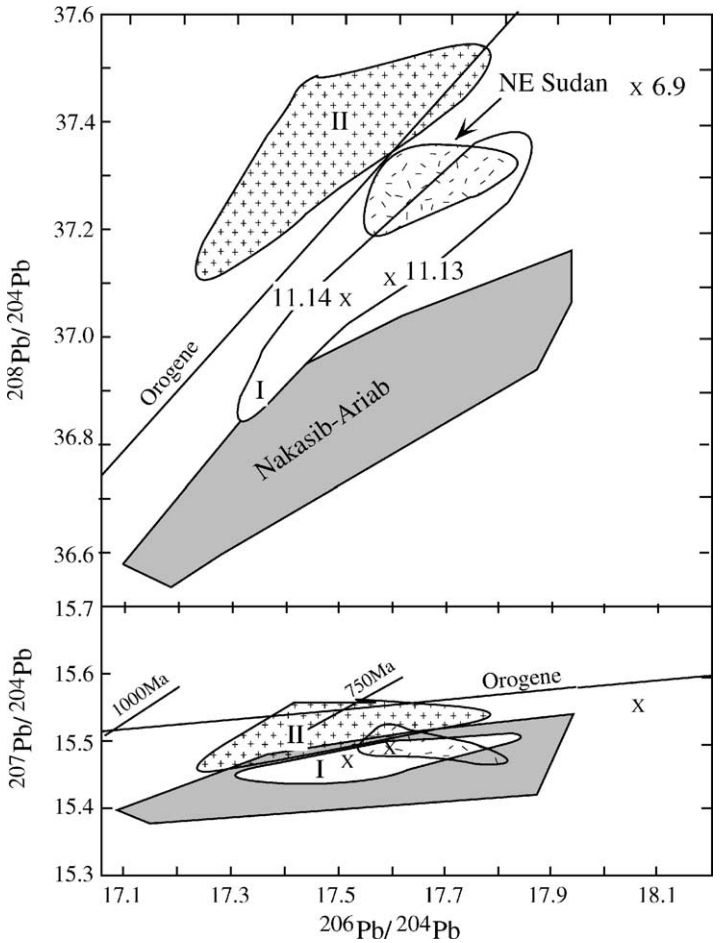

Fig. 6. Pb isotopic compositions of K-feldspars from Keraf Shear Zone samples. Fields labeled 'I' and 'II' are 'oceanic' and 'continental' fields, respectively, of Stacey et al. (1980). Trend of the 'Orogene' curve is from the plumbotectonics model of Zartman and Doe (1981). Field labeled 'NE Sudan granitoids' is for four K-feldspars from the study of Stern and Kröner (1983), and field labeled 'Nakasib-Ariab' is from Stern and Abdelsalam (1998).

for igneous rocks from eastern Sudan (Stern, 2002) and quite different from those of the Saharan Metacraton, west of the Nile (Abdelsalam et al., 2002). The similarity of Nd model age and crystallization age causes the Keraf samples to plot in the field of juvenile crust in Fig. 5B.

K-feldspars were isolated from three samples to determine their initial Pb isotopic composition (Table 6). The results are plotted in the two conventional diagrams for classification of the Pb isotopes (Stacey and Stoeser, 1983; Bokhari and Kramers, 1982; Stacey et al., 1980) (Fig. 6). In both the $^{206}Pb/^{204}Pb$ versus $^{207}Pb/^{204}Pb$ and $^{206}Pb/^{204}Pb$ versus $^{208}Pb/^{204}Pb$ diagram, the Keraf feldspars plot in or along the extension of field I (oceanic field) of Stacey et al. (1980), indicating Pb of mantle origin. It is noteworthy that sample 6.9, which is muscovite-bearing and has elevated initial $(^{87}Sr/^{86}Sr)_i$, has significantly more radiogenic $^{206}Pb/^{204}Pb$ than other samples from NE Sudan.

5. Discussion and conclusions

The data shed light on a number of interesting and important problems in the Arabian–Nubian Shield. They indicate that a major intrusive phase at about

710 Ma affected the KSZ. This age corresponds to the 'mid-Pan African Trondhjemite–Tonalite–Granodiorite Suite' (TTG Suite) identified in SE Egypt and NE Sudan (Stern and Abdelsalam, 1998), which marks widespread emplacement of 690–720 Ma intrusive rocks depleted in LIL and other incompatible trace elements. Diorites with moderately high Mg# and Ni contents are an important part of this phase in the KSZ, suggesting that mantle melting was intense as well as widespread. Two of the four samples with Sr and Y data (K39B-1, 7.15a) have high Sr/Y characteristic of adakites, also suggested by Stern and Abdelsalam (1998) to be a hallmark of the mid-Pan African TTG Suite.

The zircon evaporation ages constrain the time of sedimentation and deformation along the KSZ. Ages of 711–714 Ma for plutons intruding the Baileteb Group indicate that these metasediments must have been deposited prior to this time, and that the passive margin on the eastern flank of West Gondwana existed prior to 711–714 Ma. This is consistent with an age of ~750 Ma inferred for the carbonate rocks on the basis of Sr and C isotopic compositions (Stern et al., 1993). Similarly, the fact that these plutons were deformed during the main phase of Keraf deformation indicates that the latter is younger than 711–714 Ma. This conclusion is consistent with arguments based on regional relationships that Keraf deformation took place between 640 and 580 Ma (Abdelsalam et al., 1998). This is about the time of terminal collision between E and W Gondwana, and it is reasonable to infer that the KSZ formed in response to terminal collision.

K–Ar results indicate cooling below 325 °C occurred by about 565 Ma. This is only slightly younger than $^{40}Ar/^{39}Ar$ ages of 577 Ma from mylonitic granites in the Abu Hamed Shear Zone south of Abu Hamed (Fig. 2; Abdelsalam et al., 1998) and similar to 552–599 Ma K–Ar ages for amphibolites along the Allaqi–Heani Suture to the north (Fig. 1B; Abd El-Naby et al., 2000) and to hornblende $^{40}Ar/^{39}Ar$ ages that cluster around 580 Ma for the Hafafit and Meatiq core complexes in the Central Eastern Desert of Egypt (Fritz et al., 2002). Clearly, the basement exposed in SE Egypt and NE Sudan last was cooled below 325 °C at about 570 Ma. The cause for this cooling is not clear; it may reflect widespread erosion related to orogenic collapse of the East African Orogen (Cosca et al., 1999; Blasband et al., 2000) or oblique collision (Fritz et al., 2002). Garfunkel (1999) emphasized the importance of erosion and development of an end-Neoproterozoic peneplain in N. Africa and Arabia. The importance of extensive—perhaps global—glaciation during the Neoproterozoic is now widely appreciated (Hoffman et al., 1998). The number and timing of glaciations is still being discussed, but the end of the Neoproterozoic (550–650 Ma) was marked by two significant episodes, one (Sturtian) about 700–750 Ma and the other (Vendian) about 600 Ma (Evans, 2000). Evidence for the Sturtian glaciation is known from N. Ethiopia (Miller et al., in press) but there is no direct evidence in the ANS for Vendian glaciation. It may be that this lack of evidence for Vendian glaciation reflects the fact that this terminal Gondwana collision about this time produced a mountainous region in the interior of the end-Precambrian supercontinent, and that this supercontinent rested near the South Pole (Dalziel, 1997). The ANS at that time was probably covered by a continental ice sheet, which prohibited preservation of a sedimentary record of glaciation. In this case, K–Ar biotite ages approximate the time of unroofing associated with cutting of the Afro-Arabian peneplain by end-Neoproterozoic continental glaciation. Alternatively, a combination of orogenic collapse and glaciation may be responsible for the broad region of Africa and Arabia that is characterized by ~570 Ma K–Ar biotite ages.

The Sr, Nd, and Pb isotopic data do not reveal the presence of older crust beneath the KSZ. With one exception, Sr initial ratios are indistinguishable from those found in plutonic rocks from juvenile crust to the east. Nd isotopic data for KSZ granitoids and juvenile crust of the Arabian–Nubian Shield are indistinguishable, including for the high Sr-initial sample and the Pb feldspar data also have isotopic compositions expected for juvenile crust. These conclusions apply equally to the three intrusive rocks as well as the two gneiss samples. The isotopic data thus indicate a juvenile source for the intrusive rocks and orthogneiss, and that the eastern margin of the Saharan Metacraton must be sought farther west.

Our results are consistent with those of Küster and Liegeois (2001), who studied the basement of the NE Bayuda Desert, just to the south of the present study area (Fig. 1B). They concluded from geochemical and Sr and Nd isotopic data that the NE Bayuda basement formed at a Neoproterozic oceanic convergent

margin, with juvenile arc volcanism at 806 ± 19 Ma (Sm–Nd whole-rock isochron; $\varepsilon_{Nd(t)} = +5.2$) and T_{DM} Nd model ages of 790–900 Ma, indistinguishable from those of KSZ igneous rocks. Leucocratic gneisses and muscovite schists from farther west gave T_{DM} Nd model ages that are much older, up to 2.1 Ga. These older ages were interpreted by Küster and Liegeois (2001) to indicate derivation from an older continental source to the west.

Our data from the KSZ can be combined with the results of Küster and Liegeois (2001) to build a simplified tectonic model for the KSZ, the best window that we have into the tectonic history of the NE flank of West Gondwanaland. At about 800 Ma, an intra-oceanic arc system lay east (present co-ordinates) of older crust now known as the Saharan Metacraton. By about 730 Ma, this juvenile crust had accumulated a thick sequence of carbonate rocks on the eastern flank of this older crust. Convergent margin igneous activity may have been subdued or inactive during the interval 800–730 Ma, but flared up again about 730 Ma. Igneous activity continued until either composite terranes of the Arabian–Nubian Shield collided with this convergent margin, terminal collision between E and W Gondwanaland occurred, or both. Orogenic activity ended and the crust stabilized by about 565 Ma.

Acknowledgements

Fieldwork was conducted in 1998 and was supported by the Geological Research Authority of Sudan and the University of Juba, Sudan. We thank G. Matheis for help with XRF and ICP analyses and K. Wemmer for carrying out the K–Ar determinations. We appreciate thoughtful reviews by Hamdy Abd El-Naby and Peter Johnson. T.B.'s study at TU Berlin was sponsored by the German Academic Services (DAAD). This is UTD Geosciences Contribution #992.

References

Abd El-Naby, H., Frisch, W., Hegner, E., 2000. Evolution of the Pan-African Wadi Haimur metamorphic sole, Eastern Desert, Egypt. J. Metamorph. Geol. 18, 639–651.

Abdelrahman, E.M., 1993. Geochemical and geotectonic controls of the metallogenic evolution of selected ophiolite complexes from the Sudan. Berl. Geowiss. Abh. A 145, 175.

Abdelsalam, M.G., Stern, R.J., 1996a. Deformational history of the Neoproterozoic Keraf Zone in NE Sudan, revealed by shuttle imaging radar. J. Geol. 103, 475–491.

Abdelsalam, M.G., Stern, R.J., 1996b. Mapping Precambrian structures in the Sahara Desert with SIR-C/X-SAR radar: the Neoproterozoic Keraf Suture, NE Sudan. J. Geophys. Res. 101, 65–76.

Abdelsalam, M.G., Stern, R.J., Copeland, P., El Faki, E.M., El Hur, B., Ibrahim, F.M., 1998. The Neoproterozoic Keraf Suture in NE Sudan: sinistral transpression along the eastern margin of West Gondwana. J. Geol. 106, 133–147.

Abdelsalam, M.G., Liégeois, J.P., Stern, R.J., 2002. The Saharan Metacraton. J. Afr. Earth Sci. 34, 119–136.

Almond, D.C., Ahmed, F., 1987. Ductile shear zones in the northern Red Sea Hills, Sudan, and their implication for crustal collision. Geol. J. 22, 175–184.

Blasband, B., White, S., Brooijmans, P., De Boorder, H., Visser, W., 2000. Late Proterozoic extensional collapse in the Arabian–Nubian Shield. J. Geol. Soc. London 157, 615–628.

Bokhari, F.Y., Kramers, J.D., 1982. Lead isotopic data from massive sulfide deposits in the Saudi Arabian Shield. Econ. Geol. 77, 1766–1769.

Condie, K.C., 1998. Plate Tectonics and Crustal Evolution. Butterworth-Heinmann, Oxford, 282 pp.

Cosca, M.A., Shimron, A., Caby, R., 1999. Late Precambrian metamorphism and cooling in the Arabian–Nubian Shield petrology and $^{40}Ar/^{39}Ar$ geochronology of metamorphic rocks of the Elat area (southern Israel). Precambrian Res. 98, 107–127.

Dalziel, I.W.D., 1997. Neoproterozoic–Paleozoic geography and tectonics review, hypothesis, environmental speculation. Geol. Soc. Am. Bull. 10, 16–42.

Drummond, M.S., Defant, M.J., 1990. A model for trondhjemite–tonalite–dacite genesis and crustal growth via slab melting Archean to modern comparison. J. Geophys. Res. 95, 21503–21521.

Evans, D.A.D., 2000. Stratigraphic, geochronological, and paleomagnetic constraints upon the Neoproterozoic climatic paradox. Am. J. Sci. 300, 347–433.

Fritz, H., Dallmeyer, D.R., Wallbrecher, E., Loizenbauer, J., Hoinkes, G., Neumayr, P., Khudeir, A.A., 2002. Neoproterozoic tectonothermal evolution of the Central Eastern Desert, Egypt: a slow velocity tectonic process of core complex exhumation. J. Afr. Earth Sci. 34, 137–155.

Garfunkel, Z., 1999. History and paleogeography during the Pan-African orogen to stable platform transition reappraisal of the evidence from Elat area and the northern Arabian–Nubian Shield. Israel J. Earth Sci. 48, 135–157.

Harrison, T.M., 1981. Diffusion of ^{40}Ar in hornblende. Contrib. Mineral. Petrol. 78, 324–331.

Harrison, T.M., Duncan, I., McDougall, I., 1985. Diffusion of ^{40}Ar in biotite temperature, pressure and compositional effects. Geochim. Cosmochim. Acta 49, 2461–2468.

Irvine, T.N., Baragar, W.R.A., 1971. A guide to the chemical classification of the common volcanic rocks. Can. J. Earth Sci. 8, 523–548.

Hoffman, P.F., Kaufman, A.J., Halverson, G.P., Schrag, D.P., 1998. A Neoproterozoic snowball earth. Science 281, 1342–1346.

Kober, B., 1986. Whole-grain evaporation for $^{207}Pb/^{207}Pb$-age investigation on single zircons using a double filament thermal ion source. Contrib. Mineral. Petrol. 93, 482–490.

Kober, B., 1987. Single-zircon evaporation combined with Pb^{+} emitter bedding for $^{207}Pb/^{207}Pb$-age investigations using thermal ion mass spectrometry, and implications to zirconology. Contrib. Mineral. Petrol. 96, 63–71.

Küster, D., Harms, U., 1998. Post-collisional potassic granitoids from the southern and northwestern parts of the Late Proterozoic east African Orogeny: a review. Lithos 45, 177–195.

Küster, D., Liegeois, J.P., 2001. Isotopic and geochemical study of high-grade metamorphic lithologies from Bayuda Desert, Sudan: new insights into the Neoproterozoic evolution of the East Sahara Craton. Precambrian Res. 109, 1–23.

Miller, N.R., Alene, M., Sacci, R., Stern, R.J., Kröner, A., Conti, Zuppi, G., in press. Significance of the Tambien Group (Tigrai, N. Ethiopia) for snowball earth events in the Arabian–Nubian Shield. Precambrian Res.

Nelson, B.K., DePaolo, D.J., 1985. Rapid production of continental crust 1.7 to 1.9 b.y. ago: Nd isotopic evidence from the basement of N. America mid-continent. Geol. Soc. Am. Bull. 96, 746–754.

Pearce, J.A., Harris, N.B.W., Tindle, A.G., 1984. Trace element discrimination diagrams for the tectonic interpretation of granitic rocks. J. Petrol. 25, 956–983.

Pier, J.G., Podosek, F.A., Luhr, J.F., Brannon, J.C., Aranda-Gomez, J.J., 1989. Spinel-lherzolite-bearing quaternary volcanic centers in San Luis Potosi, Mexico; 2, Sr and Nd isotopic systematics. J. Geophys. Res. 94, 7941–7951.

Stacey, J.S., Stoeser, D.B., 1983. Distribution of oceanic and continental leads in the Arabian–Nubian Shield. Contrib. Mineral. Petrol. 84, 91–105.

Stacey, J.S., Doe, B.R., Roberts, J.R., De Levaux, M.H., Gramlich, J.W., 1980. A lead isotopic study of mineralization in the Saudi Arabian Shield. Contrib. Mineral. Petrol. 74, 175–188.

Stern, R.J., 1994. Neoproterozoic (900–550 Ma) Arc Assembly and continental collision in the East African Orogen. Ann. Rev. Earth Planet. Sci. 22, 319–351.

Stern, R.J., 2002. Crustal evolution in the East African Orogen: a neodymium isotopic perspective. J. Afr. Earth Sci. 34, 109–117.

Stern, R.J., Abdelsalam, M.G., 1998. Formation of juvenile continental crust in the Arabian–Nubian Shield: evidence from Granitic rocks of the Nakasib Suture, NE Sudan. Geol. Rundschau 87, 150–160.

Stern, R.J., Kröner, A., 1983. Late Precambrian crustal evolution in NE Sudan: isotopic and geochronologic constrains. J. Geol. 101, 555–574.

Stern, R.J., Abdelsalam, M.G., Schandelmeier, H., Sultan, M., Wickham, S., 1993. NE Sudan: a Neoproterozoic (ca. 750 Ma) passive margin on the eastern flank of West Gondwanaland. Geol. Soc. Am., Abs. Prog. 25, A49.

Zartman, R.E., Doe, B.R., 1981. Plumbotectonics the model. Tectonophysics 75, 135–162.